Dynamic Exclusion Zones for Protecting Primary Users in Database-Driven Spectrum Sharing

Sudeep Bhattarai¹⁰, Jung-Min Park¹⁰, Fellow, IEEE, and William Lehr

Abstract-In spectrum sharing, a spatial separation region is defined around a primary user (PU) where co-channel and/or adjacent channel secondary users (SUs) are not allowed to operate. This region is often called an Exclusion Zone (EZ), and it protects the PU from harmful interference caused by SUs. Unfortunately, existing methods for defining an EZ prescribe a static and an overly conservative boundary, which often leads to poor spectrum utilization efficiency. In this paper, we propose a novel framework-namely, Multi-tiered dynamic Incumbent Protection Zones (MIPZ)—for prescribing interference protection for PUs. MIPZ can be used to dynamically adjust the PU's protection boundary based on the changing radio interference environment. MIPZ can also serve as an analytical tool for quantitatively analyzing a given protection region to gain insights on and determine the trade-off between interference protection and spectrum utilization efficiency. Using results from extensive simulations and a real-world case study, we demonstrate the effectiveness of MIPZ in protecting PUs from harmful interference and in improving the overall spectrum utilization efficiency.

Index Terms—Communication networks, wireless communication, wireless networks, database systems, radio spectrum management, interference, radio propagation.

I. Introduction

N SPECTRUM sharing, two types of stakeholders share the spectrum: *incumbent users* (a.k.a. Primary Users (PUs)) and Secondary Users (SUs). PUs have exclusive access rights to their licensed spectrum whereas SUs are allowed to opportunistically access the spectrum provided that the SU-induced interference at the PU is below a predefined threshold. To ensure interference protection, a static spatial separation region is often defined around the PU where co-channel and/or adjacent-channel transmissions from SUs are not allowed. This protected region is called an Exclusion Zone (EZ). In the United States, the use of EZs is the primary exante (i.e., preventive) spectrum enforcement method that the Federal Communications Commission (FCC) and the National Telecommunications and Information Administration (NTIA) employ to protect non-federal and federal government PUs.

Manuscript received April 29, 2019; revised December 23, 2019; accepted March 11, 2020; approved by IEEE/ACM TRANSACTIONS ON NETWORKING Editor J. Xie. Date of publication April 28, 2020; date of current version August 18, 2020. This work was supported in part by the NSF under Grant 1563832, Grant 1642928, and Grant 1822173, and in part by the industry affiliates of the Broadband Wireless Access & Applications Center (BWAC). (Corresponding author: Sudeep Bhattarai.)

Sudeep Bhattarai and Jung-Min Park are with the Department of Electrical and Computer Engineering, Virginia Tech, Blacksburg, VA 24060 USA (e-mail: sbhattar@vt.edu).

William Lehr is with the Computer Science and Artificial Intelligence Laboratory (CSAIL), Massachusetts Institute of Technology (MIT), Cambridge, MA 02139 USA.

Digital Object Identifier 10.1109/TNET.2020.2986410

¹The term "Exclusion Zone" is used in this paper to refer to a spatial separation region defined for protecting PUs from SU-generated interference. We use the terms "Exclusion Zone" and "Protection Zone" interchangeably.

Defining the EZ boundary, inside which a PU enjoys exclusive spectrum access rights, is considered to be a challenging problem in spectrum sharing. The difficulty of the problem arises because of the following two conflicting requirements. On one hand, the area defined by the EZ must be sufficiently large to protect the PU from SU-induced interference. On the other hand, the EZ should not be overly large to unnecessarily limit SUs' spectrum access opportunities [3], otherwise the technological and economic viability of spectrum sharing itself is undermined. In general, the computation of EZ boundaries is based on the interference likely to be experienced by a PU; which is not just the interference caused by a single SU, but the aggregate interference from all co-existing SUs. The statistics of aggregate interference changes rapidly in a dynamic sharing scenario due to changes in SU dynamics, which complicates the design of an EZ boundary. Furthermore, when computing the EZ boundary, the effect of irregular terrain must also be considered in the path loss computations [4], which significantly increases the complexity of the already difficult problem.

Most of the existing methods for defining EZs, such as F-curves [5], consider the worst-case interference scenario and define a conservative protection boundary for the PU. In other words, they overly emphasize the protection of PUs from harmful interference [6], [7]. A good example of this can be seen in the TV bands. For example, to account for possible deep fades, the IEEE 802.22 working group specifications require detectors to have a sensitivity of -116 dBm which corresponds to an additional safety margin of roughly 20 dB (resulting in a significant increase in the size of the EZ) [8], [9]. However, in most situations, detectors do not face such severe fading, and hence SUs are unnecessarily prohibited from using the band in question even though the probability of causing harmful interference to PUs is extremely small. Thus, the legacy notion of an EZ is a static and rigid boundary that is computed by considering the worst-case interference scenario. Such overly conservative designs of EZs significantly reduce the economic benefits of spectrum sharing [10] and, in some cases, may hinder its adoption due to lack of interest from the wireless industry stakeholders.

In this paper, we propose a novel and systematic framework—namely, *Multi-tiered dynamic Incumbent Protection Zones* (MIPZ)—that can be used by a *geolocation database* (GDB)² for prescribing the protection boundaries of PUs in real-time. MIPZ ensures that PUs are protected from harmful interference by providing a *probabilistic guarantee*

1063-6692 © 2020 IEEE. Personal use is permitted, but republication/redistribution requires IEEE permission. See https://www.ieee.org/publications/rights/index.html for more information.

²A geolocation database is a network of database and supporting infrastructure that facilitates centralized management of the spectrum by collecting information from PUs and SUs, computing aggregate interference and providing real-time spectrum availability information to the SUs.

of interference protection. Unlike legacy approaches that prescribe static and overly conservative EZ boundaries, MIPZ facilitates dynamic adjustment of the PU protection boundary based on changing radio interference environment. More importantly, the protection boundaries computed by MIPZ ensure that PUs are protected from harmful interference, and, at the same time, maximize the overall spectrum utilization efficiency by providing maximum spectrum utilization opportunities for SUs. The following bullets summarize the core contributions of this paper:

- We propose a systematic framework, namely MIPZ, that can be used by GDBs for prescribing PUs' protection boundaries. These boundaries are fundamentally different from legacy EZ boundaries in that they have been designed to be dynamically adjustable based on changes in radio interference statistics and SU network dynamics.
- Based on the proposed framework, we provide closedform analytical expressions for characterizing the statistics of aggregate interference power received by a PU in GDB-driven dynamic spectrum sharing. Such systematic characterization of aggregate interference is critical in effectively protecting PUs.
- We perform extensive simulations and a real-world case study, and present results to demonstrate the effectiveness of MIPZ in ensuring interference protection to the PU and offering spectrum utilization opportunities to SUs.

It must be emphasized that the main contribution of this paper is not in the proposal of new analytical methods that are most accurate in defining EZs. Instead, our focus in on the design of a novel framework that defines dynamic EZs using analytical methods that are computationally efficient and can be implemented in real-time GDBs such as the SAS. Our work first provides a formal characterization of aggregate interference for any SU distribution in a computationally efficient manner, and then uses it in the design of MIPZ. MIPZ can be used as a computationally efficient tool for balancing the trade-off between PU protection and SU spectrum utilization efficiency. Note that other analytical methods, which are more accurate but have high computation overhead, are likely to be less practical for GDB, or even impractical, due to the computational latency and computational complexity constraints of the problem.

The rest of the paper is organized as follows. In Section II, we provide a brief technical background followed by the detailed description of MIPZ framework in Section III. The closed-form expression for the aggregate interference power is derived in Section IV. In Section V, we formulate a stochastic optimization problem for defining the dynamic EZ boundaries. Next, we demonstrate the performance of our framework by providing results from extensive simulations and a real-world case study in Sections VI and VII respectively. Finally, Section VIII concludes the paper.

II. BACKGROUND

A. Database-Driven Spectrum Sharing

With the realization that the effectiveness of dynamic spectrum sharing depends on proper spectrum management and coordination among users that share the spectrum, the FCC adopted GDB-driven spectrum sharing model in the U.S. TV bands [11]. The GDB provides centralized spectrum management among many other functionalities. The GDB has also

been mandated for enabling the three-tiered spectrum sharing model in the 3.5 GHz band [12]. Specifically, a network of GDBs and supporting infrastructure—often referred to as the Spectrum Access System (SAS)—has been mandated for enabling federal-commercial spectrum sharing in the 3.5 GHz band. The 3.5 GHz band is also known as Citizen's Broadband Radio Service (CBRS) band, and SUs that operate in the CBRS band are called Citizen's Broadband radio Service Devices (CBSDs). The SAS is a dynamic database system that computes aggregate interference on the fly and provides real-time spectrum management. It dictates how and when SUs access the spectrum. For example, when a SU sends a query for getting spectrum access, the SAS allows the SU to transmit in the co-channel only if the estimated aggregate interference at the PU is below its required interference tolerance limit.

Database Access Protocol: Database access protocol refers to a set of rules that govern how SUs and the spectrum database communicate with each other for exchanging spectrum request and response messages. Note that prescribing such a protocol is out of the scope of this paper. However, to help the reader better understand how the proposed framework works in a practical scenario, we would like to provide an excerpt of a protocol that has been proposed by WinnForum for SAS-CBSDs interaction in the CBRS band [13].

The CBSD initiates a Grant request, including CBSD identity, maximum EIRP and the desired frequency range, to the SAS. The SAS determines if the CBSD is registered and if the desired frequency range is acceptable. If so, the request is granted and the SAS responds to the CBSD that the Grant request is accepted and includes a Grant identifier, a Grant expiration time, and a heartbeat interval. The CBSD cannot use the spectrum (i.e., activate its radio transmitter) until successfully completing the CBSD Heartbeat procedure. If the SAS determines the desired operational parameters are not available for the CBSD to use, it responds to the CBSD that the Grant request is denied. As part of this response, the SAS may include a recommendation on new operational parameters for the CBSD to use. The CBSD can issue a new Grant request using the SAS recommended operational parameters.

In our work, we assume that a similar protocol exists for facilitating communication between the database and SUs, and that they use this protocol for communications pertaining to spectrum access.

B. Exclusion Zones (EZs)

An EZ is a static spatial separation region defined around a PU, where co-channel and/or adjacent-channel transmissions by SUs are prohibited. The use of EZs is the primary ex-ante mechanism employed by regulators to protect PUs from harmful interference caused by transmissions from SUs. Unfortunately, legacy EZs are overly conservative and static. The notion of a static exclusion zone implies that it has to protect PUs from the union of all likely interference scenarios, resulting in a worst-case and very conservative solution [1].

C. Aggregate Interference

When multiple SUs share the spectrum with a PU, the interference power received at the PU is not just the interference caused by a single SU, but it is the aggregate interference caused by multiple SUs. A successful design and deployment of dynamic spectrum access, therefore, requires an accurate modeling of aggregate interference. This characterization feeds into the design of protection policy for PUs (e.g., in designing EZs) and protects them from SU-generated interference.

In practical networks, a multitude of factors must be considered together in order to arrive at an accurate statistical model for the aggregate interference. Aggregate interference depends on propagation characteristics of the radio links between SUs and the PU, such as path loss, shadowing and fading, and also on the transmit power control scheme used by the SUs. Terrain characteristics in the link between the SUs and the PU also affect the distribution of aggregate interference. Furthermore, the number of SUs that transmit and their locations, themselves are random variables and affect the aggregate interference.

D. Related Work

Accurate estimation of aggregate interference is pivotal in defining effective EZ boundaries that not only adequately protect the PUs, but also enhance spectrum utilization opportunities for SUs. Therefore, researchers who work in the design and analysis of EZs primarily focus on the accurate characterization of aggregate interference. In this domain, several efforts have been made towards developing statistical models, and providing exact characterization and performance bounds for SU-generated interference [2], [14]–[16]. Prior studies have shown that models for assessing aggregate interference are not only useful for characterizing the performance of dynamic spectrum access networks, but also for designing EZs around a PU [1], [17], deploying cognitive radio networks [18], constructing radio environment maps (REMs) [19], [20], managing spectrum access control, etc.

In [21], the authors use the method of log-cumulants to approximate the distribution parameters of the aggregate interference. The authors of [22] suggest that, for arbitrarily-shaped network regions, a shifted log-normal distribution provides the overall best approximation for the aggregate interference, especially in the distribution's tail region. Reference [16] computes cummulants of aggregate interference for generating a spatial-grid-based spectrum database. However, the analysis is somewhat incomplete because it does not consider SUs' interference threshold in the design. Note that the performance of a SU may be severely impacted in the presence of interference from PU and other SUs. We consider this in our framework and facilitate a harmonious coexistence environment for both PU and SUs. Unlike in existing work, we provide quantitative results and highlight the overall technical and economic merits of using our framework under real-world conditions.

Another line of research in this domain is designing distributed systems for monitoring SU interference in real time. In [23], Ghasemi and Sousa proposed combining statistical model of interference with real-time spectrum-sensing results fed by cognitive wireless networks. Similarly, a concept called SMAP (distributed spectrum management architecture and protocol) is proposed in [24] with the intention of enabling wireless devices and networks to coordinate their spectrum use through an Internet-based common spectrum control plane. Gao *et al.* [25] propose a mechanism for incentivizing SUs to participate in spectrum sensing, the result of which augments spectrum database by defining smaller EZs with dynamic

boundaries and creating additional spectrum access opportunities for SUs. While EZ refinement based on sensing results offers great merits and has the potential to significantly reduce the size of EZs in real-time, it comes with a huge cost: deploying sensing network, and setting-up an infrastructure for data collection and processing is expensive. Furthermore, sensing results collected from participatory nodes/sensors are only useful if they come with precise geo-locations, but doing so puts both PUs' and SUs' privacy at risk [26]. Our work addresses these concerns as it does not require the installation of sensing nodes and the collection of sensitive information from SUs.

III. PROPOSED FRAMEWORK: MULTI-TIERED DYNAMIC INCUMBENT PROTECTION ZONES (MIPZ)

A. Motivation and Objective

One of the primary limitations of conventional EZs is that they are overly large. The EZ boundary is defined conservatively so that PUs are protected from interference even in the worst-case scenario. The conservative approach for defining the conventional EZ boundary is backed up by the following fact. Outside the EZ, existing spectrum sharing models do not specify the limit on the number of simultaneous co-channel SU transmissions—i.e., any SU can transmit in the co-channel as long as it is outside the PU's EZ. Thus, the interference power received at the PU is the aggregate interference caused by all such co-existing SUs. Naturally, in the absence of a real-time spectrum access controller, regulators have to set large EZ boundaries for ensuring that PUs are protected from harmful interference even in the worst-case scenario.

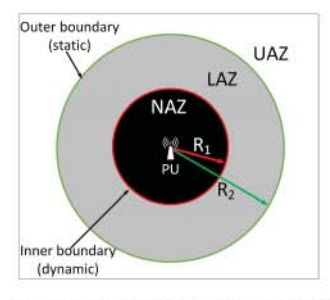
The FCC in its NPRM [12] acknowledges that the size of an EZ could be significantly reduced if there were a mechanism for controlling the number of SU transmissions outside the EZ. The introduction of GDB-driven spectrum sharing, such as SAS in the 3.5 GHz band, is an initiative towards this direction. The SAS framework allows regulators to tightly control access to the spectrum by modeling the statistics of aggregate interference at the PU in real-time. Motivated by this initiative, we propose MIPZ for prescribing EZs of PUs in GDB-driven spectrum sharing. MIPZ allows the spectrum controller to adjust the size of the EZ dynamically based on instantaneous interference conditions, and hence, allows SUs to exploit more spectrum opportunities than the legacy EZs while still providing sufficient interference protection to PUs.

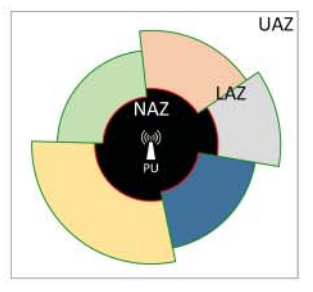
B. Conceptual Design

MIPZ is composed of three access zones around the PU, each of which has a different degree of spectrum access restriction based on its proximity to the PU. A GDB enforces this differential spectrum access hierarchy to provide spectrum availability information to the SUs.

The three access zones defined by MIPZ are:

1) No Access Zone (NAZ): NAZ is the spatial region defined in the immediate vicinity of the PU. Due to its proximity to the PU, even a single SU transmission in this region causes harmful interference to the PU. Therefore, SUs located in the NAZ region are not allowed to access the spectrum—any SU that sends a spectrum query to the GDB with an intent to operate inside the NAZ receives a denial.





(a) Concept of NAZ, LAZ and UAZ (b) Realizing irregular PZs using annular sectors

Fig. 1. MIPZ design.

- 2) Limited Access Zone (LAZ): LAZ is the spatial region that lies just outside the NAZ. It is relatively far from the PU, and hence, it is safe to allow a few SUs to transmit in this region without causing harmful interference to the PU. However, it is not far enough for allowing any number of SUs to transmit; otherwise, the aggregate interference power from all SUs will significantly deteriorate the performance of PU. Therefore, MIPZ allows only a limited number of co-channel SUs, say N, to transmit simultaneously in the LAZ region.
- 3) Unlimited Access Zone (UAZ): UAZ is the region that lies outside the LAZ. Essentially, this region is similar to the area outside conventional EZs where any number of SUs can transmit in the co-channel. Since the UAZ lies far from the PU, the effective interference caused by SUs that operate in this region is negligible due to large path loss. Thus, the MIPZ model allows SUs to have unencumbered access to the co-channel in the UAZ.

The conceptual design of MIPZ is illustrated in Figure 1(a). The PU is located at the center and SUs are spread around the PU in different access zones. Notice that the two zones boundaries: i) inner boundary, and ii) outer boundary are key elements in defining NAZ, LAZ and UAZ regions. The outer boundary is defined to be static while the inner boundary is made to be dynamically adjustable based on changes in radio interference statistics, spectrum demand and/or SU transmission parameters. We shall discuss the details of these boundary definitions in Section V.

C. Assumptions and Design Constraints

In practice, the zone boundaries will not always be perfect circles as shown in Figure 1(a). Terrain variations, environmental effects, antenna radiation pattern, etc. cause the radio signal to attenuate differently in different directions resulting in irregular zone boundaries. To consider irregularities of zone boundaries, we adopt a sectorized model as shown in Figure 1. We assume that the area within an annular sector exhibits similar propagation characteristics. Here, each annular sector is a part of LAZ while the inner black irregular shape represents the NAZ. The radius of the inner boundary, as well as N, needs to be defined for each LAZ sector. We believe that this sectorized model strikes an appropriate compromise between modeling realistic propagation environment and limiting modeling complexity.

We assume that SUs in each LAZ sector are uniformly distributed—i.e., the location of a SU is a two-dimensional uniform random variable. At first, this assumption might seem impractical as several studies have shown that mobile

users tend to be clustered due to geographical factors, social gatherings, etc [27], [28]. However, although SUs are assumed to be distributed uniformly in a LAZ sector, we do not imply that they are distributed uniformly around the PU. Similar to piece-wise linear models that are often used to approximate a curve, we use piece-wise uniform distribution to model an arbitrary SU distribution. Admittedly, MIPZ framework has the inherent ability to approximate any SU distribution by considering different SU density in each LAZ sector. This is one of the core strengths of our model.

For protection of PUs from harmful interference, we assume that a PU can operate without significant performance degradation if it is ensured a probabilistic guarantee of interference protection. More precisely, a PU achieves its quality of service (QoS) if the aggregate interference (I_{agg}) from SUs is lessthan-or-equal-to a threshold, say I_{th} , for at least $(1-\epsilon)$ fraction of the time, where ϵ is a pre-defined probabilistic threshold.

$$P\left(I_{agg} \le I_{th}\right) \ge 1 - \epsilon. \tag{1}$$

Since radio propagation is unpredictable, the notion of probabilistic-interference-protection-guarantee is common in wireless applications. For example, the coverage regions of TV stations are based on F-curves which provide probabilistic guarantees that the signal reception is above a threshold.

When multiple SUs operate in the LAZ region, coexistence among SUs is a concern. In our design, for simplicity and for the sake of analytical tractability, we assume that SUs can harmoniously coexist without causing harmful interference to each other as long as the density of SUs (number of SUs per unit area) does not exceed a threshold. The SU-SU coexistence in the UAZ region is, however, out of the scope of this paper.

Henceforth, we assume that the PU has a co-located transmitter (Tx) and receiver (Rx) unless explicitly stated otherwise, and focus the design of MIPZ boundaries for co-located PUs. Examples of co-located PUs are satellite earth stations, radar systems, etc. Later, in Section V, we shall provide insights on how to apply/extend MIPZ for non-co-located PUs.

When SUs share the spectrum with a PU that transmits with high power (e.g., satellite Earth stations, radars, etc.), the interference from PU to SU is also a concern. This needs to be considered while defining the NAZ and LAZ regions. For instance, although allowing a low-power SU to operate near the PU may not affect PU's performance, it may not be feasible for the SU to operate near the PU due to large interference power from the PU.

Lastly, it must be emphasized that the primary constraint in MIPZ design is the protection of PU from harmful interference. In the next section, we focus on modeling the statistics of aggregate interference caused by SUs to the PU in the MIPZ framework. The discussions in the next section will lay the foundation for defining the MIPZ boundaries in Section V.

IV. AGGREGATE INTERFERENCE AT THE PU

In this section, we derive an expression for the probability distribution of aggregate interference experienced by the PU due to transmissions from multiple SUs.

Since SUs are prohibitted inside NAZ, the NAZ region does not contribute to interference at the PU. Also, SUs in the UAZ have negligible contribution to the aggregate interference because of large path loss. Thus, the aggregate interference power experienced by the PU is the summation of interference caused by N SUs in the LAZ region. Let us start with modeling the co-channel interference measured at a PU that is caused by a single SU operating in a LAZ sector.

A. Interference From a Single SU

Let us consider a single SU operating inside a LAZ sector. For computing the path loss between a SU and a PU, let us consider a simplified propagation model with exponential path loss and shadowing. We choose this path loss model for the following two reasons: i) it is a popular path loss model used for modeling large-scale outdoor channels, and has also been extensively used by prior 3GPP standards bodies [29], and ii) it facilitates us in deriving a closed-form analytical expression for the aggregate interference.

Beyond a reference distance d_0 , the dB path loss (P_L) in the channel that links the SU and the PU is,

$$P_L = a + b \log_{10} d + \psi, \tag{2}$$

where $a=P_L(d_0)-b\log_{10}d_0$, $P_L(d_0)$ is the mean path loss at the reference distance in dB, $b=10\gamma$, γ is the path loss exponent, d is the distance between a SU and the PU in meters, and ψ is the log-normal (normal in log scale) shadowing coefficient with zero mean and variance $=\sigma^2$. From here onwards, we shall consider all computations in log scale unless explicitly stated otherwise; therefore, whenever we say normal distribution, it is actually a normal distribution in the log scale and a log-normal distribution in the absolute scale.

Let P_{ts} denote the transmit power of SU in dBm. Then, the interference power received by the PU receiver is,

$$I_{SU} = P_{ts} - P_L$$

= $P_{ts} - (a + b \log_{10} d + \psi)$. (3)

Suppose that SUs are uniformly distributed in an annular sector and the PU is located at the center of the circle that forms the annular sector. Then the distance between a SU and the PU can be represented with a random variable D whose probability density function (pdf) is given by Equation (4) [30].

$$f_D(d) = \frac{2d}{R_2^2 - R_1^2}, \quad R_1 \le d \le R_2.$$
 (4)

Here, R_1 and R_2 represent the radii of the inner and outer concentric circles, respectively, which combinedly define the annular LAZ sector.

Since ψ is a normal random variable, its pdf is,

$$f_{\psi}(\psi) = \frac{1}{\sqrt{2\pi}\sigma} e^{-\frac{\psi^2}{2\sigma^2}}.$$
 (5)

Finally, using convolution integral [31] and properties of transformation of random variables, the pdf of I_{SU} , denoted as $f_{ISU}(i_{su})$, can be derived (see Appendix A).

$$\begin{split} f_{I_{SU}}(i_{su}) &= Ke^{\left(\frac{2(P_{ts}-i_{su}-a)\ln 10}{b}\right)} \left\{ erf(B) - erf(A) \right\}, \quad (6) \\ \text{where } K &= \frac{\ln 10}{b(R_2^2-R_1^2)} e^{\frac{2(\ln 10)^2\sigma^2}{b^2}} \\ A &= \frac{1}{\sqrt{2}\sigma} \left(P_{ts} - i_{su} - a - b\log_{10}R_2 + \frac{2\sigma^2\ln 10}{b} \right) \\ \text{and } B &= \frac{1}{\sqrt{2}\sigma} \left(P_{ts} - i_{su} - a - b\log_{10}R_1 + \frac{2\sigma^2\ln 10}{b} \right) \end{split}$$

As mentioned before, Equation (6) is valid for any SU operating in any LAZ sector. When specific values of a,b,P_{ts},σ,R_1 and R_2 pertaining to i^{th} SU operating in j^{th} LAZ sector are plugged into Equation (6), the pdf of $I_{SU_{i,j}}$ is obtained. Here, $I_{SU_{i,j}}$ denotes the pdf of interference power at the PU receiver due to the transmission from i^{th} SU operating in a randomly chosen location inside the j^{th} LAZ sector.

Observation 1: For small ω , where $\omega = \frac{R_2}{R_1}$, the pdf of I_{SU} can be approximated as a log-normal distribution. The error in approximation increases monotonically with ω .

Proof: Let us rewrite equation (6) as follows,

$$f_{I_{SU}}(i_{su}) = K'g_1(i_{su})g_2(i_{su}),$$
 (7)

where $g_2(i_{su}) = erf(g_3(i_{su})) - erf\left(g_3(i_{su}) - \frac{b \log_{10} \omega}{\sqrt{2}\sigma}\right)$, and $g_3(i_{su})$ and $g_1(i_{su})$ are linear and exponential functions of i_{su} respectively. Here, K' is a non-negative constant.

From the definition of the erf function, the plot of $g_2(i_{su})$ can be approximated as a Gaussian pdf. This approximation is fairly accurate when $\frac{b \log_{10} \omega}{\sqrt{2}\sigma}$ is small. Restating this in terms of our design parameter ω , the Gaussian approximation holds true only for small values of ω .

Finally, using the fact that the product of an exponential kernel $(g_1(i_{su}))$ has the kernel of an exponential distribution) and a Gaussian kernel (based on the above discussion, $g_2(i_{su})$ has the kernel of a Gaussian distribution) results in an another Gaussian kernel, $f_{ISU}(i_{su})$ is a Gaussian pdf.

The Gaussian approximation for the plot of $g_2(i_{su})$ is highly accurate when ω is small. However, as ω becomes larger, the bell shaped curve of $g_2(i_{su})$ starts to deviate from the Gaussian pdf. Figure 2(a) shows the comparative plots of $g_2(i_{su})$ against the closest normal pdf for different values of ω . Large values of ω causes $g_2(i_{su})$ (and $f_{I_{SU}}(i_{su})$) to deviate from the normal pdf resulting in a non-zero approximation error (ΔI_{SU}). Here, ΔI_{SU} is defined as the *Kullback-Leibler (K-L) divergence* between actual and approximated distributions of I_{SU} denoted by $I_{SU}^{(\text{actual})}$ and $I_{SU}^{(\text{approx.})}$ respectively. We use K-L divergence because it precisely captures the information-based measure of disparity among probability distributions and has been used extensively in the literature in similar contexts [32].

$$\Delta I_{SU} = \sum_{i} I_{SU}^{(\text{actual})}(i) * \log \left(\frac{I_{SU}^{\text{actual}}(i)}{I_{SU}^{\text{approx.}}(i)} \right).$$

In Figure 2(b), the actual plot of $f_{I_{SU}}(i_{su})$ from Equation (6) and its complementary cumulative distribution function (ccdf) are compared against the pdf and the ccdf of normal approximation respectively. For generating these plots, typical practical values were used for all other variables ($a=37~\mathrm{dB}$, b=20, $\sigma=3$, $P_{ts}=23~\mathrm{dBm}$, $R_2=126~\mathrm{km}$). Then, the parameters of the normal approximation are obtained by fitting a least-squares normal curve to the samples of $f_{I_{SU}}(i_{su})$. We can observe a close similarity between the two pdfs, especially when ω is small. The plot of ΔI_{SU} in Figure 2(c) shows that ΔI_{SU} increases with increase in ω . As expected, the approximation error is a function of ω but not of the actual values of R_1 and R_2 . Another important observation is that for any ω , ΔI_{SU} increases as the ratio γ/σ increases. Therefore, in general, ΔI_{SU} increases as the term $\left(\frac{b \log_{10} \omega}{\sqrt{2}\sigma}\right)$ increases. In practical implementation of MIPZ, the value of ω is not

In practical implementation of MIPZ, the value of ω is not significantly large. For instance, when $R_2=126$ km, R_1

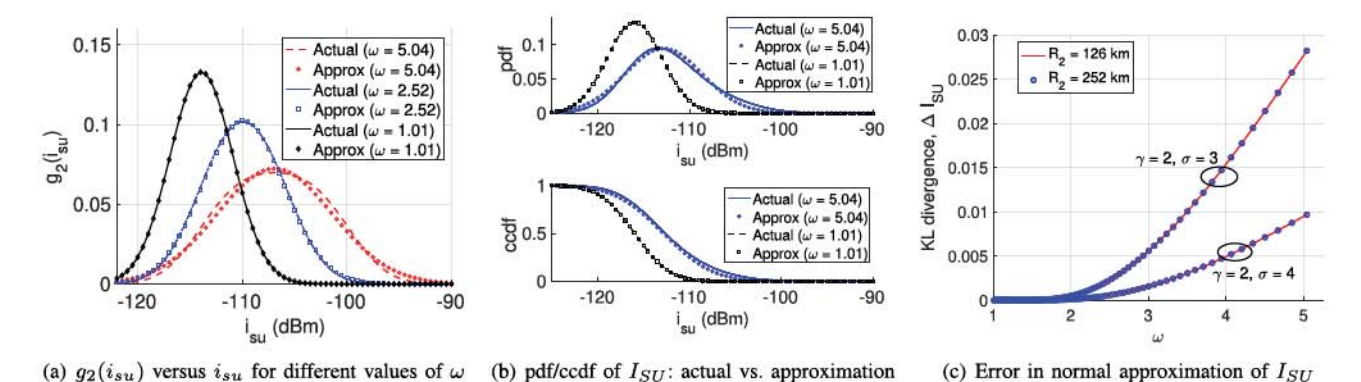


Fig. 2. Approximating the distribution of an SU-generated interference as a standard normal (Gaussian) distribution.

ranges from 50 km to 126 km, which implies ω ranges from 1 to 2.52. At this value, ΔI_{SU} is fairly negligible. Later, we shall provide results and show that this approximation does not have unfavorable consequences on the overall performance of PU and SU networks.

B. Aggregate Interference

The next step is to find the distribution of aggregate interference, I_{agg} , which is a sum of random variables, $I_{SU_{i,j}}$.

$$I_{agg} = \sum_{j=1}^{T} \sum_{i=1}^{N_j} I_{SU_{i,j}}.$$
 (8)

Here, T denotes the total number of LAZ sectors and N_j is the total number of SUs operating in the j^{th} LAZ sector. Note that Equation (8) is valid in standard units (Watts or milliWatts), but not in log scale. Since the distribution of $I_{SU_{i,j}}$ (in standard units) is log-normal, I_{agg} has the distribution of summation of log-normal random variables.

It has been shown that the summation of log-normal random variables can be approximated by another log-normal [33]. Several approximation techniques have been proposed [33], [34]. The most widely used approximations are the ones proposed by Fenton-Wilkinson [35], Schwartz-Yeh [36] and Mehta et al. [37]. Fenton-Wilkinson provides a simple and computationally efficient algorithm for approximating the mean and variance of the resulting log-normal distribution. While it provides a very good approximation in the tail region of the cdf curve, Fenton-Wilkinson is usually bad in the body region. Schwartz-Yeh provides a good approximation in the body region at the cost of added computational complexity, but unlike Fenton-Wilkinson, it doesn't do well in the tail region. Mehta et. al. provide a flexible mechanism that allows a user to choose the region in which the approximation is most accurate. However, its computational complexity increases exponentially with increase in number of random variables being summed, which makes it the least favorable for using in real-time large network applications like the SAS.

From inequality (1), it is clear that we are interested in the tail portion of the ccdf of I_{agg} . Fenton-Wilkinson fits our purpose because it provides a log-normal approximation that is most accurate in the tail region [38]. Moreover, it performs well even with the summation of non-identically distributed log-normal variables (summands). This is desired in our case because the distribution of I_{SU} might be different

for different LAZ sectors when sectors have different sets of parameters such as γ , P_{ts} and σ . Furthermore, Fenton-Wilkinson provides a closed-form solution for the mean and variance of the resulting log-normal distribution, making it easier to implement in the SAS. The closed-form solutions are given in Equations (9) and (10) [35].

$$\sigma_{agg}^{2} = \ln \left(\frac{\sum_{j=1}^{T} \sum_{i=1}^{N_{j}} \left(e^{2\mu_{i,j} + \sigma_{i,j}^{2}} \left(e^{\sigma_{i,j}^{2}} - 1 \right) \right)}{\sum_{j=1}^{T} \sum_{i=1}^{N_{j}} \left(e^{\mu_{i,j} + \frac{\sigma_{i,j}^{2}}{2}} \right)} + 1 \right)$$
(9)

$$\mu_{agg} = \ln \left(\sum_{j=1}^{T} \sum_{i=1}^{N_j} \left(e^{\mu_{i,j} + \frac{\sigma_{i,j}^2}{2}} \right) \right) - \frac{\sigma_{agg}^2}{2}, \tag{10}$$

where $\mu_{i,j}$ and $\sigma_{i,j}^2$ denote the mean and variance of individual summand. Similarly, μ_{agg} and σ_{agg}^2 are mean and variance of the resulting log-normal distribution; I_{agg} in our case.

The above equations are valid for natural logarithm, and they must be scaled appropriately when working with other logarithms (\log_{10} in our case).

V. DETERMINING THE MIPZ BOUNDARIES

Recall that MIPZ defines NAZ, LAZ and UAZ regions based on two boundaries: outer and inner boundaries. In this section, we leverage our findings from the previous section and describe a methodology for defining these boundaries.

A. Static Outer Boundary

The spectrum sharing etiquette in the UAZ region is exactly the same as that in the region outside a conventional EZ. The SAS provides unencumbered access to the co-channel in the UAZ which forces us to define the outer boundary conservatively, just like the conventional EZ boundary. Otherwise, the PU may not be guaranteed an adequate interference protection either due to line-of-sight interference from peak points in some terrain areas, or due to the aggregate interference from SUs. However, there might be some spectrum access opportunities near the conventional EZ boundary which are unnecessarily thwarted because of conservative boundary definition. To exploit such opportunities, we leverage the conventional EZ boundary definition as a starting point and use it as the outer boundary of our framework, and then explore spectrum opportunities inside it. This also allows us to make

a direct comparison between the conventional EZ and MIPZ in terms of spectrum utilization.

We define the outer boundary of our framework in the same way regulators define conventional EZ boundaries, i.e., based on the maximum distance at which the PU can get interference from the SUs. The maximum distance depends on several factors such as SU transmit power, type of modulation and coding, PU Rx antenna gain, PU's interference protection and QoS requirement, etc. We assume that the outer boundary is static and fixed because it is computed based on the worst-case interference scenario.

B. Dynamic Inner Boundary

In MIPZ framework, only a limited number of SUs are allowed to operate in the LAZ region. Usually, wireless network conditions are dynamic: for example, during peak times of the day, a large number of SUs send requests to access the channel, while during maintenance hours, only a few of them do so. For maximizing the overall spectrum utilization efficiency, it is desired that the size of the LAZ region be adjusted dynamically based on spectrum demand, network dynamics and aggregate-interference statistics. For instance, when SU density is high, LAZ should be smaller in size and lie far from the PU to ensure adequate protection. Therefore, we define the inner boundary dynamically based on changing network dynamics and radio-interference environment. This makes the LAZ region flexible in size which adapts its inner boundary based on changing network dynamics.

Now, let us define the upper and lower bounds of R_1 , the inner boundary. Clearly, the upper bound of R_1 is the outer boundary R_2 . When $R_1 = R_2$, our model becomes equivalent to the conventional EZ. When $R_1 < R_2$, there is a non-zero area available in the LAZ region. This is where MIPZ allows a limited number of SUs, say N, to operate. Small R_1 implies large area in the LAZ region, and apparently, it seems that this translates to a higher value of N. However, small R_1 has two major implications. The first issue with small R_1 is that it results in large ΔI_{SU} . Figure 2(b) shows that our approximation predicts lower probability of interference in the tail region as compared to that given by the exact closedform expression of I_{SU} . As R_1 gets smaller, this difference increases. The implication is that when R_1 is small and our approximation is used to compute the available number of spectrum resources, N, in the LAZ, it computes N that is larger than the actual N that should have been permitted in the LAZ had the approximations been not used. This endangers the PU's interference protection, and therefore, forces us to define a lower bound on R_1 , say $R_{1lb}^{(1)}$.

Recall that the approximation error ΔI_{SU} increases with ω . Therefore, for ensuring protection of PU from interference, ΔI_{SU} must be constrained below a threshold, say $\Delta I_{SU}^{\rm th}$. The first step in computing $R_{1lb}^{(1)}$ is to plot a curve similar to that shown in Figure 2(c) for a given propagation environment (note that γ and σ define the propagation environment), and then choosing the maximum value of ω (say $\omega_{\rm max}$) where $\Delta I_{SU} \leq \Delta I_{SU}^{\rm th}$. Finally, $R_{1lb}^{(1)}$ is computed as $R_{1lb}^{(1)} = \frac{R_2}{\omega_{\rm max}}$. Another issue with small R_1 is that it brings the LAZ region

Another issue with small R_1 is that it brings the LAZ region closer to the PU. Referring to Figure 2(b), small R_1 causes the I_{SU} ccdf to shift to the right, and increases the probability

that $I_{SU} > I_{th}$ for any given value of I_{th} . This forces us to define another lower bound for R_1 , say $R_{1_{lb}}^{(2)}$, based on the interference protection requirement of the PU. $R_{1_{lb}}^{(2)}$ is the distance at which a single SU endangers the protection requirement of the PU. It is calculated using I_{th} , ϵ and pathloss equations.

When PU-Tx and PU-Rx are co-located, $R_{1lb}^{(2)}$ depends on the interference from SU for a desired interference protection requirement of the PU. We define the interference tolerance level of PU in terms of outage probability, which is the probability that the received signal power coming from a co-channel SU is greater than a predefined interference threshold. The outage probability at the PU due to interference from a co-channel SU located at $R_{1lb}^{(2)}$ in a shadow fading channel with variance = σ^2 is calculated as follows,

$$\epsilon = P\left(I_{SU} \ge I_{th}\right) = Q\left(\frac{I_{th} - \bar{I}_{SU}}{\sigma}\right)$$
(11)

where Q(.) is the Gaussian Q function, and \bar{I}_{SU} is the mean interference power which is given by,

$$\bar{I}_{SU} = P_{ts} - a - 10\gamma \log_{10} R_{1lb}^{(2)}, \tag{12}$$

where $a=10\gamma log_{10}\left(\frac{4\pi f}{c}\right)$, f is the radio frequency and c is the speed of propagation of the radio wave through the medium. Plugging (12) in (11) and rearranging gives $R_{1b}^{(2)}$.

$$R_{1_{lh}}^{(2)} = 10^{\left(\frac{\sigma Q^{-1}(\epsilon) + P_{ts} - a - I_{th}}{10\gamma}\right)}.$$
 (13)

Some co-located PUs, such as radars and satellite Earth stations, have significantly higher transmit power (upto 90 dBm) compared to that of SUs (20 – 33 dBm for the small cell LTE base stations) [39]. When there is a large power discrepancy between the PU and the SU, the interference from the PU to the SU is a concern. To incorporate this in our framework, we introduce a third lower bound on R_1 , say $R_{1tb}^{(3)}$. $R_{1tb}^{(3)}$ is the minimum distance from the PU at which a SU can achieve its desired QoS level. If the QoS of a SU is also defined in terms of probabilistic guarantee of interference protection, $R_{1tb}^{(3)}$ is given by equation (13) when I_{th} and ϵ are replaced with the interference threshold and outage probability of the SU, and P_{ts} is replaced with the transmit power of the PU

Now, the smallest R_1 that satisfies all three bounds is R_{min} .

$$R_{min} = \max\left(R_{1_{lb}}^{(1)}, R_{1_{lb}}^{(2)}, R_{1_{lb}}^{(3)}\right). \tag{14}$$

When R_1 is large, the LAZ region lies far from the PU-Rx. The ccdf curve of Figure 2(b) shifts to the left. From this, we expect to achieve large N. However, large R_1 means small area for spectrum sharing in the LAZ region, and to address the co-existence issues among SUs, N should be small. These conflicting requirements make the problem of defining the inner boundary challenging.

Let λ denote the total number of spectrum requests coming from uniformly distributed SUs in an area between R_{min} and R_2 of a LAZ sector. Then, the total number of spectrum requests in an annular region between R_1 and R_2 , λ_{LAZ} , is,

$$\lambda_{LAZ} = \frac{\lambda (R_2^2 - R_1^2)}{(R_2^2 - R_{min}^2)}. (15)$$

To account for SU-SU coexistence, suppose that a maximum of ρ SUs can co-exist in the area between R_{min} and R_2 . From here onwards, we shall use the term "SU" to refer to a SU cell with a Tx at the center and a single Rx at the cell edge. In practice, the value of ρ depends on SU's coverage area, its transmit power, required Signal-to-Noise-and-Interference-Ratio (SINR) at the SU-Rx, antenna parameters, path loss exponent and shadow fading environment. For abstracting away these details and for simplicity, let us assume that coexistence is a function of the total area available for SUs and the area of each SU cell. Define $\rho = \frac{(R_2^2 - R_{min}^2)}{r_{su}^2}$, where r_{su} is the cell radius of the SU. Then, the total number of SUs that can co-exist in an area between R_1 and R_2 , ρ_{LAZ} , is,

$$\rho_{LAZ} = \frac{(R_2^2 - R_1^2)}{r_{su}^2}. (16)$$

Ideally, the desired number of SUs in the LAZ region is the minimum of λ_{LAZ} and ρ_{LAZ} . There is no incentive in allowing more than λ_{LAZ} SUs because only λ_{LAZ} spectrum requests are originated from the LAZ region. Also, allowing more than ρ_{LAZ} SUs causes harmful co-existence interference among SUs.

Based on above discussions, we formulate the following stochastic optimization problem for finding optimum R_1 that maximizes N while minimizing ω , and also satisfies the PU's protection criteria. Recall that minimizing ω ensures that the approximation error, ΔI_{SU} , is minimized. In this formulation, it is assumed that there is a single LAZ sector and SUs operating in the LAZ have different transmission parameters, resulting in different distribution of I_{SU} (denoted by I_{SU_i} for each SU.

$$\begin{aligned} \text{Maximize}: & \alpha N - \omega \\ \text{subject to}: & P\left(\sum_{i=1}^{N} I_{SU_i} \leq I_{th}\right) \geq 1 - \epsilon \\ & R_{min} \leq R_1 \leq R_2 \\ & 0 \leq N \leq \min(\lambda_{LAZ}, \rho_{LAZ}). \end{aligned} \tag{17}$$

Here, α is a scaling factor that can be used to prioritize spectrum utilization over approximation error or vice-versa. The designer can carefully choose this parameter to balance the trade-off between spectrum efficiency and design error.

Now, let us extend the above problem formulation to the case where there are T LAZ sectors. Suppose $N^{(j)}$, $R_{min}^{(j)}$, $R_1^{(j)}$, $R_2^{(j)}$, $\lambda_{LAZ}^{(j)}$ and $\rho_{LAZ}^{(j)}$ denote the number of SUs, R_{min} , R_1 , R_2 , λ_{LAZ} and ρ_{LAZ} of the j^{th} sector respectively. Similarly, let $I_{SU_{ij}}$ denote the I_{SU} of i^{th} SU operating in the j^{th} LAZ sector. Then, the optimization problem (17) can be reformulated as (18).

$$\begin{split} \text{Maximize}: & \ \sum_{j=1}^T \left(\alpha \eta^{(j)} N^{(j)} - \omega\right) \\ \text{subject to}: & \ P\left(\sum_{j=1}^T \sum_{i=1}^{N^{(j)}} I_{SU_{ij}} \leq I_{th}\right) \geq 1 - \epsilon \\ & \ R_{min}^{(j)} \leq R_1^{(j)} \leq R_2^{(j)}, \quad j = 1 \dots T \\ & \ 0 \leq N^{(j)} \leq \min(\lambda_{LAZ}^{(j)}, \rho_{LAZ}^{(j)}), \quad j = 1 \dots T, \end{split}$$

When all SUs within a LAZ sector have the same link capacity (Mbps/Hz), the weights $\eta^{(j)}$ correspond to the relative spectral capacities (or relative spectral efficiencies) of SUs in different LAZ sectors. It is advantageous to have a large number of SUs in the sector that has higher link capacity for each SU. Link capacities can be different when different types of SUs (e.g., LTE, WiFi, etc.) or SUs with different operating parameters (e.g., P_{ts} , r_{su} , etc.) operate in different LAZ sectors. Terrain characteristics, which might be different in different LAZ sectors, affect the propagation characteristics, γ and σ , which in turn affect the link capacities of SUs.

Optimization problems (17) and (18) are mixed-integer non-linear programming problems as they require $N^{(j)}$, $j=1\ldots T$ to be integers and the interference constraint is nonlinear. Several algorithms such as cutting-plane [40] and branch-and-bound [41] can be used to solve this kind of problems. But often, due to their computational complexity, *Genetic Algorithm* (GA) is preferred. A GA is a heuristic search algorithm for solutions of optimization problems that starts from a random initial guess and attempts to find the best solution under some criteria [42]. Problems (17) and (18) can be easily solved using GAs.

In practice, λ , ρ and other operational parameters of PU and SU vary with time. Changes in these parameters cause the distributions of $I_{SU_{ij}}$ and I_{agg} to change. The SAS regularly computes the optimum values of R_1 and N based on changing network dynamics and uses it to respond to SUs' queries. In real-world implementation of MIPZ, when the LAZ of multiple PUs overlap, interference from all SUs that lie in the overlapping LAZ region must be considered in the computation of aggregate interference for each PU.

Heretofore, we have assumed that PUs have co-located Tx and Rx. However, in practice, PUs may have a non-co-located Tx and a Rx, such as the case in point-to-point radio links and broadcast systems. It is noteworthy that our derivations can easily be applied to non-co-located single-point PU links (i.e., one PU-Tx and one PU-Rx separated by a certain distance) as long as interference computations are done correctly. In particular, when computing the interference from SU to PU (used for computing I_{agg} and $R_{1lb}^{(2)}$), the distance between SU and PU-Rx must be used for estimating the path loss. On the other hand, while computing the interference from PU to SU (used for computing $R_{1lb}^{(3)}$), the distance between PU-Tx and SU must be taken into account. The NAZ, LAZ and UAZ regions are defined around the PU-Rx.

When the PU is a broadcast system that comprises of a single Tx and multiple Rxs spread over a region, our derivations can be extended as follows. The centroid of all PU-Rx locations becomes the center of the NAZ, LAZ and UAZ region. We can now assume that a virtual PU-Rx is located at the centroid. Then, zone boundaries are computed by considering $I_{th} - \Delta I$ (both in log units) as the interference protection threshold of the virtual PU, where ΔI is the interference margin computed using path loss between the farthest PU-Rx and the virtual PU-Rx.

VI. SIMULATION RESULTS

In this section, we present simulation results for demonstrating the performance of MIPZ framework. In the first half of this section, we compare results from our analysis

to those from Monte-Carlo simulations, and justify that the normal approximation for characterizing the pdf of I_{SU} has negligible impact on the PU's interference protection. Then, in the later half, we present results to show that our framework dynamically adjusts the size of the LAZ, computes the maximum allowable number of SUs in the LAZ based on changing network dynamics, and maximizes the overall spectrum utilization.

Let us define a database coverage region as a 300 km by 300 km square, where a single PU is located at the center. Suppose that the PU is a high-power station, such as a satellite earth station, and its transmit power, the interference tolerance threshold (I_{th}) and the probabilistic threshold for interference protection (ϵ) are 60 dBm, -100 dBm and 0.1 respectively, unless otherwise explicitly stated. Following NTIA's definitions of EZs for protecting satellite earth stations, let us assume that us assume that the EZ defined to protect this PU from harmful interference from SUs is a circular region of 126 km [43]. Hence, in the MIPZ framework, we set $R_2 = 126$ km.

Let us also assume that all SUs are commercial LTE cells, each comprising of a base station and multiple UEs. Recent studies have shown that there is no effect on the throughput of LTE-cells when the interference power from a co-existing PU is below -50 dBm [44]. Therefore, we assume that for proper operation of SUs, the interference from the PU should be below -50 dBm at least 0.9 fraction of the time. Using this, the minimum required distance between the PU and a SU is computed and used as one of the lower bounds in Equation (14).

Furthermore, for simplicity and without the loss of generality, let us assume that the LAZ consists of a single annular region whose propagation characteristics is governed by Equation (2). Other simulation parameters are outlined in Table I. The optimization problem (17) is solved in Matlab's GA solver using these parameter values, and optimum values of R_1 and N are computed. Finally, we use these results to study the performance of PU and SU networks in terms of interference protection and spectrum utilization respectively.

A. PU Interference Protection: Our Approximation Versus Monte-Carlo Simulations

The closed-form expression for I_{agg} was derived based on the following two approximations: i) pdf of I_{SU} (in standard units) is log-normal, and ii) sum of log-normals is another log-normal. In order to justify that the PU's interference protection is not compromised by making these approximations, we perform a Monte-Carlo (MC) based simulation study and compare the distribution of I_{agg} obtained from MC simulations to that from our model.

First, let us assume that the actual path loss of a link is defined by Equation (2). Then, using our approximations made in Section IV for characterizing the distribution of aggregate interference and by solving the optimization problem (18), the optimum values of R_1 and N are computed. Finally, the distribution of I_{agg} obtained from this analytical study is plotted.

For the MC analysis, we perform 50,000 simulation runs. In each simulation run, i) N SUs (obtained from the solution of optimization problem (17)) are uniformly distributed in the LAZ region (i.e., the area between R_1 and R_2), and

TABLE I
SAMPLE PARAMETERS FOR SIMULATIONS

| Radio frequency, f | 1755 MHz ³ |
|---|-----------------------|
| Radiation pattern | Omnidirectional |
| SU transmit power, P_{ts} | 23 dBm |
| SU cell size, r_{su} | 2 km |
| Total spectrum requests from SUs, λ | 10,000 |
| Channel bandwidth (W_s) | 15 MHz |
| Path loss exponent, γ | 2 |
| Standard deviation of shadow fading, σ | 3 dB |

TABLE II
FOUR SCENARIOS CONSIDERED IN FIGURE 3

| Scenario | γ | σ (dB) | P_{ts} (dB) |
|----------|----------|--------|---------------|
| 1 | 2.5 | 4 | 35 |
| 2 | 2.5 | 7 | 35 |
| 3 | 2 | 4 | 23 |
| 4 | 2 | 7 | 23 |

ii) the aggregate interference power received at the PU is calculated using Equations (3) and (8). By repeating steps i) and ii), the actual empirical distribution of I_{agg} is obtained. Finally, we compare the distribution of I_{agg} obtained from MC simulations against the one obtained from closed-form expressions given by our model. Figure 3 shows a close similarity between the two plots for different scenarios outlined in Table II. Our model approximates the actual distribution of I_{aqq} fairly precisely, especially in the tail region of the ccdf curve. This validates the correctness of our approximation in that it does not compromise the interference protection of the PU. In other words, even with our approximation, the probabilistic guarantee of interference protection, $P(I_{agg} \leq I_{th} \text{ dBm}) \geq$ $1-\epsilon$, is always achieved. However, it is noteworthy that our approximation slightly underestimates I_{agg} for large γ and small σ values, and slightly overestimates it for small γ and large σ values.

B. Spectrum Utilization: Adapting to Network Dynamics

To study the effect of several network parameters on SU spectrum utilization, we first need to define a metric for quantifying SU spectrum utilization. Let us define spectrum utilization in terms of $Area\ Sum\ Capacity\ (ASC)$, which is the sum of channel capacity values of each co-existing SU within the database coverage area. Throughout the simulations, we assume that a SU refers to a LTE-cell of radius r_{su} , which comprises of a base station at the center and a UE at the cell edge. The channel capacity (C_{SU}) of a SU operating in a channel of bandwidth W_s Hz is calculated using the Shannon capacity formula.

$$C_{SU} = W_s log_2(1 + SINR) \tag{19}$$

Here, the SINR at the SU-Rx is given by,

$$SINR = \frac{P_{ts}/P_L(r_{su})}{n_s W_s + I_{P2S} + I_{S2S}}$$
 (20)

where, $P_L(r_{su})$ is the path loss between the SU-Tx and the SU-Rx, n_s is the thermal noise power at the SU-Rx, I_{P2S} is the interference power at the SU caused by transmissions

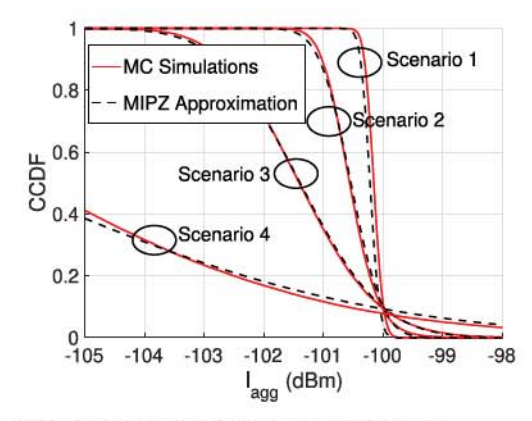


Fig. 3. ccdf of aggregate interference experienced by PU.

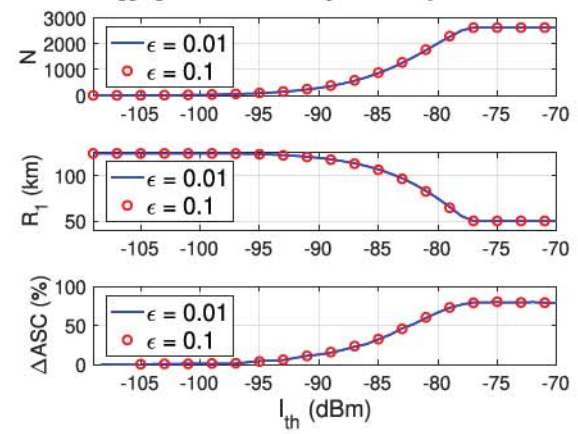


Fig. 4. Effect of I_{th} on N, R_1 and Δ ASC.

from the PU and I_{S2S} is the aggregate interference power at the SU from other co-existing SUs.

Now, if we assume all SUs operate in the same channel, the total SU ASC (in bits per second) is computed as,

$$ASC = W_s \sum_{i=1}^{N_T} log_2(1 + SINR_i)$$
 (21)

where, N_T represents the total number of SUs in the system (both LAZ and UAZ), and SINR $_i$ denotes the SINR at the i^{th} SU-Rx.

1) Effect of I_{th} : To study the effect of I_{th} and ϵ on N, R_1 and ASC, we fix the values of all other parameters and solve optimization problem (18) for different values of I_{th} and ϵ . The results are summarized in Figure 4. As seen from the plots, when I_{th} increases, SAS extends the LAZ region towards the PU by making R_1 smaller until it becomes equal to R_{min} . Increased area in the LAZ due to high I_{th} implies that more SUs (increased N) can be allowed. Although the increased number of SUs in the LAZ lowers the SINR of existing SUs in both UAZ and LAZ regions due to increased I_{S2S} and decreases their capacity, Figure 4 shows that the ASC gain from additional SUs is significant enough to overcome the loss. Another observation in Figure 4 is that around $I_{th} =$ -77 dBm, R_{min} kicks in and does not allow R_1 to decrease further even when I_{th} increases. Also, since the upper bound of N depends on R_1 (recall the last constraint of optimization problem (18)), N saturates and so does ASC.

Another important observation in Figure 4 is the low sensitivity of N on ϵ . In this particular scenario, the resulting distribution of I_{agg} has small variance, and hence, the tail

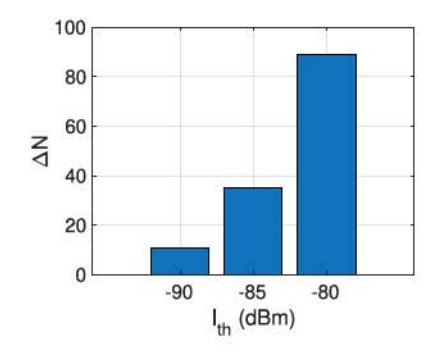


Fig. 5. Effect of ϵ on N. Here, ΔN denotes the difference in N computed using $\epsilon=0.1$ and $\epsilon=0.01$.

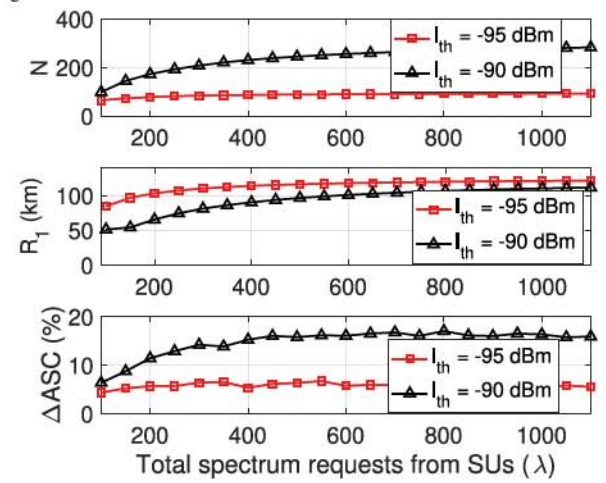


Fig. 6. Effect of λ on N, R_1 and Δ ASC.

region of the CCDF curve falls sharply (similar to Scenario 1 of Figure 3). Therefore, we do not see a significant change in N even when ϵ changes by an order of magnitude. However, when the distribution of I_{agg} has large variance, such as the case in Scenario 4, N increases with an increase in ϵ . This is shown in Figure 5. In the figure, ΔN is defined as $N_{\epsilon=0.1}-N_{\epsilon=0.01}$, where $N_{\epsilon=0.1}$ and $N_{\epsilon=0.01}$ denote the value of N computed for $\epsilon=0.1$ and $\epsilon=0.01$ respectively. Aligning with our intuition, $N_{\epsilon=0.1}>N_{\epsilon=0.01}$ and ΔN increases with I_{th} because MIPZ can allow more SUs to coexist in the band when the PU is less sensitive to interference.

- 2) Effect of λ : The effect of λ on N, R_1 and ASC is shown in Figure 6 for different I_{th} values at $\epsilon=0.1$. When there are less number of SU requests, the SAS maximizes N by increasing the size of the LAZ, i.e., making R_1 smaller. Small λ implies small λ_{LAZ} , therefore, the upper bound on N is limited by λ_{LAZ} , but not ρ_{LAZ} (recall the last constraint of (17)). Consequently, increasing λ_{LAZ} by decreasing R_1 maximizes N, and hence, the ASC. However, the lower bound on R_1 prevents the SAS from decreasing it below R_{min} as noticed in Figure 6 for $I_{th}=-90$ dBm. Another observation from Figure 6 is that $R_{1_{lb}}^{(2)}$ for sensitive PUs (PUs that have small I_{th}) is large, and this results in large R_{min} . Large R_{min} implies small λ_{LAZ} which results in smaller N, and hence, a smaller gain in ASC as compared to the less sensitive PUs.
- 3) Effect of r_{su} : Figure 7 shows how MIPZ adapts to the change in SU cell size, r_{su} , and addresses the co-existence among SUs in the LAZ. From Equations (16) and (18), it is clear that large r_{su} reduces ρ_{LAZ} , a factor that dictates the upper bound of N. Therefore, N is small when r_{su} is

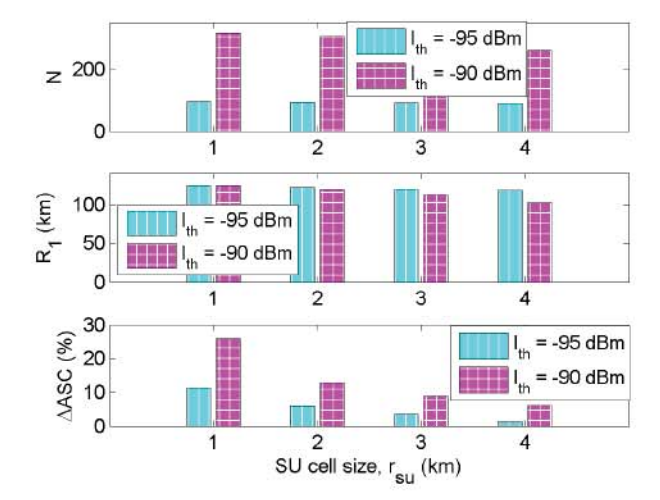


Fig. 7. Effect of r_{su} on N, R_1 and ΔASC .

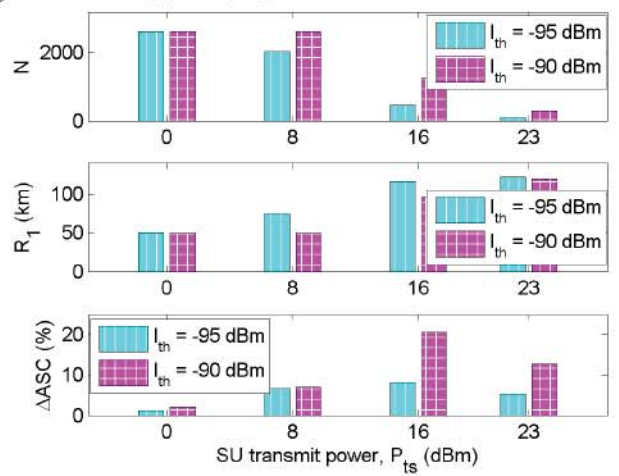


Fig. 8. Effect of P_{ts} on N, R_1 and ΔASC .

large. The SAS tries to compensate this by increasing the area of the LAZ region (by reducing R_1) and allowing SUs to operate closer to the PU. However, decreasing R_1 below a certain value is not permitted because of the PU's interference protection requirement. Another observation in Figure 7 is that ASC decreases more sharply than N when r_{su} increases. Recalling our assumption that each SU cell consists of a transmitter at the center and a receiver at the cell edge, a large r_{su} implies reduced SINR at the SU-Rx, hence the result.

4) Effect of P_{ts} : MIPZ also adapts to the change in P_{ts} of SUs operating in the LAZ. The results are summarized in Figure 8. When P_{ts} is high, the SAS forces SUs to operate far from the PU by increasing R_1 . Large R_1 implies small λ_{LAZ} and ρ_{LAZ} , the upper bounds on N. As a result, N is small. Nevertheless, this decrease in N does not necessarily reduce the ASC. With high P_{ts} , SU Rxs in the LAZ experience increased SINR due to less interference from other SUs, which results in a gain in ASC. From the plots, we can notice that this gain overcomes the loss in ASC due to decreased N. Figure 8 also provides us a valuable insight that P_{ts} can be optimized for maximizing the ASC.

VII. APPLICATION OF MIPZ: A CASE STUDY

In this section, we present a case study that demonstrates the applicability of MIPZ in real-world spectrum sharing.



Fig. 9. Illustration of the region considered in our case study.

The PU considered in this study is an actual MetSat Earth station that operates in the AWS-3 band and is located near the Petuxant River in Maryland, USA. To protect this Earth station from harmful interference, the NTIA has defined a circular EZ of radius 126 km [43]. Note that the area outside this circular EZ corresponds to the UAZ region of MIPZ, and hence, we set R_2 to to 126 km. The location of the PU as well as the area covered by its EZ (dotted curve) is shown in Figure 9. It is noteworthy that such a conservative definition of an EZ prohibits highly-populated regions such as Washington DC, Baltimore and Richmond from getting access to the shared spectrum. Therefore, in this study, we aim to answer the following question: Given the operational parameters of PU and SUs, is it possible for the SAS to allow a limited number of SUs to co-exist inside the EZ boundary without compromising the interference protection requirement of the PU?

More specifically, our interest is in finding the maximum number of co-channel SUs, N, that can be allowed to operate in Washington and Baltimore, as shown in the green annular sector of Figure 9. Instead of computing optimum values of both N and R_1 , here we fix R_1 (i.e., pre-define the LAZ region), and compute the optimum value of N. Finally, we validate our results by comparing against actual solutions obtained by using the Irregular Terrain Model (ITM) in point-to-point (PTP) mode.

Using ITM-PTP, the value of N that satisfies Inequality (11) can be computed by following these steps:

- For an entrant SU querying from a random location within LAZ, use ITM-PTP path loss model—using precise geo-locations of PU and SU, and a terrain database for extracting terrain elevation data—to estimate the path loss from the SU to the PU.
- Use SU transmission parameters and path loss computed in step 1 to compute the interference power at the PU.
- 3. Repeat above steps for all entrant SUs one by one and allow SUs to access the spectrum if I_{agg} is less than I_{th} . Also, allow, with probability ϵ , the first SU—that causes I_{agg} to exceed I_{th} —to access the spectrum. Prohibit all other SUs from getting access to the shared spectrum.
- 4. Count the total number of SUs, N, that are allowed to access the spectrum.

The above steps can be repeated to obtain the distribution of I_{agg} and the mean value of N, which are compared against the ones obtained using our MIPZ framework.

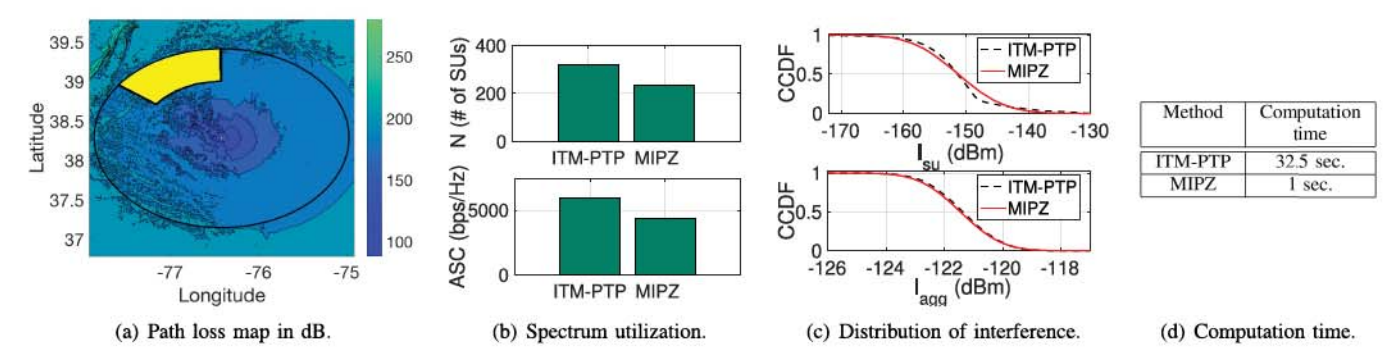


Fig. 10. Summary of results from our case study.

A. PU Protection and Spectrum Utilization Efficiency

The results from our case study are summarized in Figure 10. Figure 10(a), shows the path loss map generated by computing the ITM-PTP path loss from the center of each grid to the PU (located at the center). The terrain details required in the ITM-PTP path loss computations were extracted from the Global Land One-km Base Elevation (GLOBE) database [45]. Notice the EZ and the LAZ from Figure 9 are also overlaid on top of the path loss map. The black oval and the yellowish annular sector represent the EZ boundary and the LAZ region, respectively.

Figure 10(c), compares the probability distribution of I_{SU} and I_{agg} . For MIPZ, the parameters γ and σ of the simplified path loss model are estimated by fitting a least-squares curve to the samples obtained from ITM-PTP path loss samples. Using the fitted parameters, MIPZ computes the optimum value of N. Finally, the distribution of I_{agg} estimated by MIPZ is compared against the actual I_{agg} distribution obtained by using ITM-PTP path loss values. Clearly, we can see the results overlap, which indicates that "When proper values of γ and σ are used, MIPZ provides the same level of interference protection guarantee to the PU as that provided by the ITM-PTP model".

Figure 10(b), demonstrates the effectiveness of MIPZ in enabling spatial sharing opportunities for SUs. MIPZ identifies spatial sharing opportunities by estimating N (and ASC), almost as effectively as the ITM-PTP model. A slight underperformance of MIPZ, as compared against the ITM-PTP mode, is attributed to the fact that MIPZ uses statistics of radio path loss whereas ITM-PTP considers the actual obstructions in the link for computing the path loss (and hence, interference). Despite this slight disadvantage, MIPZ has a clear advantage over the ITM-PTP based method in terms of the following two aspects:

Computation time: While the ITM-PTP based method is computationally expensive, MIPZ is computationally efficient. The former method requires us to compute path loss values from each SU to the PU whereas MIPZ approximates I_{agg} using closed-form analytical expressions. Moreover, MIPZ is scalable because its computation time is a constant (approx. one second in our implementation), unlike ITM PTP whose computation complexity grows proportionally with N. In particular, the computational complexity of the ITM-PTP based method is $O(N \times \tau)$, where $O(\tau)$ is the time complexity of each ITM-PTP path loss computation (approx. 100 milliseconds in our implementation). The exact computation times for both methods are reported in Figure 10(d).

Knowledge of the SU's precise geolocation: MIPZ does not require precise geolocations of SUs; it only needs to know whether a SU lies inside a LAZ sector. On the other hand, the ITM-PTP based method requires the precise geolocations of SUs which, in some cases, might not be available. For example, the SAS may not know the SUs' precise geolocations due to SUs' mobility or because of location privacy concerns (the location privacy of SUs is also a serious concern in database-driven spectrum sharing). In such cases, ITM-PTP cannot be used to accurately compute the I_{agg} caused by SUs.

B. Economic Impact of Employing MIPZ

Referring to Figure 9, here we discuss the possible economic merit of MIPZ. The outer boundary represents the current EZ defined by NTIA [43] for a AWS-3 based MetSat Earth station, and the green annular region is the LAZ region defined by MIPZ. The introduction of the LAZ region serves approximately 10 million people of Washington D.C. and Baltimore, MD, which would otherwise lie in the NTIA-defined EZ. With a bandwidth of 15 MHz, this area represents about 150 million MHz-POPs million MHz-POPs for a wireless operator. Using Verizon's valuation of the nearby AWS band in their proposed spectrum swap, this is worth approximately \$132 million per auction period [3], [46]. As expected in spectrum the actual economic value largely depends on how near or far the PU is from densely populated areas.

VIII. CONCLUSION

In this paper, we introduced the concept of multi-tiered dynamic EZs for prescribing interference protection to PUs in GDB-driven spectrum sharing. The proposed framework allows a limited number of SUs to operate closer to the PU, and improves the overall spectrum utilization while ensuring a probabilistic guarantee of interference protection to the PUs. By making some reasonable assumptions, we derived a closed-form expression of the aggregate interference power received by the PU, and used it to dynamically adjust the size of the EZ boundary. Using results from extensive simulations and a real-world case study, we showed that our framework defines more effective and dynamic EZs that not only protect PUs from harmful interference, but also improve the overall spectrum utilization efficiency.

APPENDIX

A. Derivation of Equation (6)

The pdf of the second term of equation (2) can be obtained by using the transformation of random variable

 $D \text{ to } Y, y = b \log_{10} d = g(d).$

$$f_Y(y) = f_D(g^{-1}(y)) \left| \frac{\partial g^{-1}(y)}{\partial y} \right|$$

= $\frac{2 \ln{(10)} 10^{2y/b}}{b(R_2^2 - R_1^2)}$, $b \log_{10} R_1 \le y \le b \log_{10} R_2$.

Also, the pdf of $Z = Y + \psi$ can be obtained by using the convolution integral formula [31],

$$f_Z(z) = \int_{A_1}^{B_1} \frac{1}{\sqrt{2\pi}\sigma} e^{-\frac{\psi^2}{2\sigma^2}} \frac{2\ln(10)10^{2(z-\psi)/b}}{b(R_2^2 - R_1^2)} d\psi,$$

where $A_1=z-b\log_{10}R_2$ and $B_1=z-b\log_{10}R_1$. Let $K_1=\sqrt{\frac{2}{\pi}}\frac{\ln 10}{\sigma b(R_2^2-R_1^2)}$ and proceed.

$$f_Z(z) = K_1 \int_{A_1}^{B_1} e^{-\frac{\psi^2}{2\sigma^2}} e^{\frac{2(z-\psi)\ln 10}{b}} d\psi$$

$$= K_1 e^{\left(\frac{2z\ln 10}{b} + \frac{2(\ln 10)^2\sigma^2}{b^2}\right)} \int_{A_2}^{B_2} e^{-\frac{1}{2}\frac{k^2}{\sigma^2}} dk, \quad (22)$$

where $k=\psi+\frac{2\sigma^2\ln 10}{b},\ A_2=z-b\log_{10}R_2+\frac{2\sigma^2\ln 10}{b}$ and $B_2=z-b\log_{10}R_1+\frac{2\sigma^2\ln 10}{b}.$

Letting $p=\frac{k}{\sqrt{2}\sigma}$ and $K=\frac{\ln 10}{b(R_2^2-R_1^2)}e^{\frac{2(\ln 10)^2\sigma^2}{b^2}}$, equation (22) becomes,

$$f_{Z}(z) = \frac{2}{\sqrt{\pi}} K e^{\left(\frac{2z \ln 10}{b}\right)} \int_{A_{3}}^{B_{3}} e^{-p^{2}} dp$$

$$= K e^{\left(\frac{2z \ln 10}{b}\right)} \left\{ erf(B_{3}) - erf(A_{3}) \right\},$$
where $erf(x) = \frac{2}{\sqrt{\pi}} \int_{0}^{x} e^{-p^{2}} dp,$

$$A_{3} = \frac{1}{\sqrt{2}\sigma} \left(z - b \log_{10} R_{2} + \frac{2\sigma^{2} \ln 10}{b} \right), \text{ and}$$

$$B_{3} = \frac{1}{\sqrt{2}\sigma} \left(z - b \log_{10} R_{1} + \frac{2\sigma^{2} \ln 10}{b} \right).$$

Finally, the pdf of P_L in equation (2) is obtained.

$$f_{P_L}(p_l) = Ke^{\left(\frac{2(p_l - a)\ln 10}{b}\right)} \left\{ erf(B_4) - erf(A_4) \right\}, \quad (23)$$
 where $A_4 = \frac{1}{\sqrt{2}\sigma} \left(p_l - a - b\log_{10}R_2 + \frac{2\sigma^2\ln 10}{b} \right), \text{ and}$
$$B_4 = \frac{1}{\sqrt{2}\sigma} \left(p_l - a - b\log_{10}R_1 + \frac{2\sigma^2\ln 10}{b} \right).$$

Using equations (23) and (3), the pdf of I_{SU} is given by,

$$\begin{split} f_{I_{SU}}(i_{su}) &= Ke^{\left(\frac{2(P_{ts}-i_{su}-a)\ln 10}{b}\right)} \left\{ erf(B) - erf(A) \right\}, \\ \text{where } A &= \frac{1}{\sqrt{2}\sigma} \left(P_{ts}-i_{su}-a-b\log_{10}R_2 + \frac{2\sigma^2\ln 10}{b} \right) \\ \text{and } B &= \frac{1}{\sqrt{2}\sigma} \left(P_{ts}-i_{su}-a-b\log_{10}R_1 + \frac{2\sigma^2\ln 10}{b} \right) \end{split}$$

REFERENCES

- S. Bhattarai, A. Ullah, J.-M.-J. Park, J. H. Reed, D. Gurney, and B. Gao, "Defining incumbent protection zones on the fly: Dynamic boundaries for spectrum sharing," in *Proc. IEEE Int. Symp. Dyn. Spectr. Access* Netw. (DySPAN), Sep. 2015.
- [2] S. Bhattarai, J.-M. Jerry Park, W. Lehr, and B. Gao, "TESSO: An analytical tool for characterizing aggregate interference and enabling spatial spectrum sharing," in *Proc. IEEE Int. Symp. Dyn. Spectr. Access Netw. (DySPAN)*, Mar. 2017, pp. 1–10.
- [3] M. Altamimi and M. B. H. Weiss, "Enforcement and network capacity in spectrum sharing: Quantifying the benefits of different enforcement scenarios," in *Proc. 41st Res. Conf. Commun., Inf. Internet Policy*, Mar. 2014, pp. 1–38.
- [4] R. Murty, R. Chandra, T. Moscibroda, and P. Bahl, "SenseLess: A database-driven white spaces network," *IEEE Trans. Mobile Comput.*, vol. 11, no. 2, pp. 189–203, Feb. 2012.
- [5] R. A. O'Connor, "Understanding television's grade A and grade B service contours," *IEEE Trans. Broadcast.*, vol. 47, no. 3, pp. 309–314, Sep. 2001.
- [6] M. Vu, N. Devroye, and V. Tarokh, "On the primary exclusive region of cognitive networks," *IEEE Trans. Wireless Commun.*, vol. 8, no. 7, pp. 3380–3385, Jul. 2009.
- [7] S. Kusaladharma and C. Tellambura, "Aggregate interference analysis for underlay cognitive radio networks," *IEEE Wireless Commun. Lett.*, vol. 1, no. 6, pp. 641–644, Dec. 2012.
- [8] S. J. Shellhammer, S. S. N, R. Tandra, and J. Tomcik, "Performance of power detector sensors of DTV signals in IEEE 802.22 WRANs," in *Proc. 1st Int. Workshop Technol. Policy Accessing Spectr. (TAPAS)*, 2006, p. 4-es.
- [9] R. Tandra, A. Sahai, and S. M. Mishra, "What is a spectrum hole and what does it take to recognize one?" *Proc. IEEE*, vol. 97, no. 5, pp. 824–848, May 2009.
- [10] Report to the President Realizing the Full Potential of Government-Held Spectrum to Spur Economic Growth, PCAST, Washington, DC, USA, Jul. 2012.
- [11] Second Report and Order and Memorandum Opinion and Order, document (FCC 08-260), FCC, Nov. 2008.
- [12] Report and Order and Second Further Notice of Proposed Rulemaking, document GN Docket 12-354, FCC, Apr. 2015.
- [13] Signaling Protocols and Procedures for Citizens Broadband Radio Service (CBRS): Spectrum Access System (SAS)—Citizens Broadband Radio Service Device (CBSD) Interface Technical Specification, document WINNF-16-S-0016, Wireless Innovation Forum, WinnForum, Dec. 2016.
- [14] M. Labib, A. F. Martone, V. Marojevic, J. H. Reed, and A. I. Zaghloul, "A stochastic optimization approach for spectrum sharing of radar and LTE systems," *IEEE Access*, vol. 7, pp. 60814–60826, 2019.
- [15] S. Bhattarai, J.-M. Park, B. Gao, K. Bian, and W. Lehr, "An overview of dynamic spectrum sharing: Ongoing initiatives, challenges, and a roadmap for future research," *IEEE Trans. Cognit. Commun. Netw.*, vol. 2, no. 2, pp. 110–128, Jun. 2016.
- [16] S. Yamashita, K. Yamamoto, T. Nishio, and M. Morikura, "Exclusive region design for spatial grid-based spectrum database: A stochastic geometry approach," *IEEE Access*, vol. 6, pp. 24443–24451, 2018.
- [17] M. S. Ali and N. B. Mehta, "Modeling time-varying aggregate interference from cognitive radios and implications on primary exclusive zone design," in *Proc. IEEE Global Commun. Conf. (GLOBECOM)*, Dec. 2013, pp. 3760–3765.
- [18] M. F. Hanif, M. Shafi, P. J. Smith, and P. Dmochowski, "Interference and deployment issues for cognitive radio systems in shadowing environments," in *Proc. IEEE Int. Conf. Commun.*, Jun. 2009, pp. 1–6.
- [19] H. Yilmaz, T. Tugcu, F. Alagöz, and S. Bayhan, "Radio environment map as enabler for practical cognitive radio networks," *IEEE Commun. Mag.*, vol. 51, no. 12, pp. 162–169, Dec. 2013.
- [20] Y. Hu and R. Zhang, "Secure crowdsourced radio environment map construction," in *Proc. IEEE 25th Int. Conf. Netw. Protocols (ICNP)*, Oct. 2017, pp. 1–10.
- [21] G. Pastor, I. Mora-Jimenez, A. J. Caamano, and R. Jantti, "Log-cumulant matching approximation of heavy-tailed-distributed aggregate interference," in *Proc. IEEE Int. Conf. Commun. (ICC)*, Jun. 2015, pp. 4811–4815.
- [22] J. Guo, S. Durrani, and X. Zhou, "Characterization of aggregate interference in arbitrarily-shaped underlay cognitive networks," in *Proc. IEEE Global Commun. Conf.*, Dec. 2014, pp. 961–966.

- [23] A. Ghasemi and E. S. Sousa, "Interference aggregation in spectrumsensing cognitive wireless networks," IEEE J. Sel. Topics Signal Process., vol. 2, no. 1, pp. 41-56, Feb. 2008.
- [24] P. Karimi, W. Lehr, I. Seskar, and D. Raychaudhuri, "SMAP: A scalable and distributed architecture for dynamic spectrum management," in Proc. IEEE Int. Symp. Dyn. Spectr. Access Netw. (DySPAN), Oct. 2018, pp. 1-10.
- [25] B. Gao et al., "Incentivizing spectrum sensing in database-driven dynamic spectrum sharing," in Proc. IEEE 35th Annu. IEEE Int. Conf. Comput. Commun. (INFOCOM), Apr. 2016, pp. 1–9.
 [26] CBRS Operational Security, document WINNF-TS-0071, WinnForum,
- Jul. 2017.
- [27] V. D. Blondel, A. Decuyper, and G. Krings, "A survey of results on mobile phone datasets analysis," EPJ Data Sci., vol. 4, no. 1, p. 10, Dec. 2015.
- [28] M. Haenggi and R. K. Santi, Interference in Large Wireless Networks, 1st ed. Boston, MA, USA: Now, Nov. 2009.
- [29] T. S. Rappaport, R. W. Heath, Jr., R. C. Daniels, and J. N. Murdock, Millimeter Wave Wireless Communications, 2nd ed. Upper Saddle River, NJ, USA: Prentice-Hall, 2014.
- [30] S. Sinanovic, H. Burchardt, H. Haas, and G. Auer, "Sum rate increase via variable interference protection," IEEE Trans. Mobile Comput., vol. 11, no. 12, pp. 2121-2132, Dec. 2012.
- [31] O. Ibe, Fundamentals of Applied Probability and Random Processes. Amsterdam, The Netherlands: Elsevier, 2014.
- [32] S. Kullback and R. A. Leibler, "On information and sufficiency," Ann. Math. Statist., vol. 22, no. 1, pp. 79-86, 1951. [Online]. Available: http://www.jstor.org/stable/2236703
- [33] S. Asmussen, J. Jensen, and L. Rojas-Nandapaya, "A literature review on lognormal sums," Tech. Rep. [Online]. Available: http://citeseerx.ist. psu.edu/viewdoc/download?doi=10.1.1.719.5927&rep=rep1&type=pdf
- [34] B. R. Cobb and R. Rumi, "Approximating the distribution of a sum of log-normal random variables," in Proc. 6th Eur. Workshop Probabilistic
- Graph. Models, 2012, pp. 1–8.
 [35] L. Fenton, "The sum of log-normal probability distributions in scatter transmission systems," IEEE Trans. Commun., vol. 8, no. 1, pp. 57-67,
- [36] S. C. Schwartz and Y. S. Yeh, "On the distribution function and moments of power sums with log-normal components," Bell Syst. Tech. J., vol. 61, no. 7, pp. 1441-1462, Sep. 1982.
- N. Mehta, J. Wu, A. Molisch, and J. Zhang, "Approximating a sum of random variables with a lognormal," IEEE Trans. Wireless Commun., vol. 6, no. 7, pp. 2690-2699, Jul. 2007.
- [38] N. C. Beaulieu and Q. Xie, "An optimal lognormal approximation to lognormal sum distributions," IEEE Trans. Veh. Technol., vol. 53, no. 2,
- pp. 479–489, Mar. 2004.
 [39] F. Rayal, "The hype and reality of small cells performance," Cisco, San Jose, CA, USA, Tech. Rep., Feb. 2012. [Online]. Available: https://community.cisco.com/t5/service-providers-blogs/the-hypereality-of-small-cells-performance/ba-p/3664738
- [40] K.-D. Chen, Z. Wu, and Z.-J. Xia, "A new cutting plane algorithm for integer linear programming," in Proc. Int. Conf. Comput. Sci. Service Syst., Aug. 2012.
- [41] J. Eckstein, "Control strategies for parallel mixed integer branch and bound," in Proc. ACM/IEEE Conf. Supercomput., Nov. 1994, pp. 41-48.
- [42] T. Yokota and M. Gen, "Solving for nonlinear integer programming problem using genetic algorithm and its application," in Proc. IEEE Int. Conf. Syst., Man Cybern., vol. 2, Oct. 1994, pp. 1602-1609.
- [43] Coordination Procedures in the 1695-1710 MHz, and 1755-1780 MHz, Bands, document (FCC 13-185), FCC and NTIA, Jul. 2014.
- [44] M. Juskauskas et al., "Experimental investigation of radar interference into LTE system at 1800 MHz frequency band," in Proc. 21st Telecommun. Forum Telfor (TELFOR), Nov. 2013, pp. 28-30.
- [45] NOAA. The Global Land One-km Base Elevation Project. Accessed: Mar. 25, 2016. [Online]. Available: http://www.ngdc.noaa.gov/mgg/ topo/globe.html
- [46] K. D. Gordon et al., A Review of Approaches to Sharing or Relinquishing Agency-Assigned Spectrum, document P-5102, Science and Technology Policy Institute, Jan. 2014.



Sudeep Bhattarai received the bachelor's degree in electronics and communications engineering from Tribhuvan University, Nepal, in 2011, the master's degree in electrical engineering from Tennessee State University, USA, in 2013, and the Ph.D. degree in electrical and computer engineering from Virginia Tech, USA, in 2018. He is currently a Wireless Software Engineer at Apple Inc. His research interests include dynamic spectrum sharing and access, coexistence among heterogeneous wireless technologies, advanced wireless networks, and operational privacy

and security issues in wireless communications. He was a recipient of the Best Paper Award at the IEEE DySPAN 2014 and a Finalist of the Paul E. Torgersen Graduate Student Research Excellence Award at Virginia Tech.



Jung-Min (Jerry) Park (Fellow, IEEE) received the Ph.D. degree in electrical and computer engineering from Purdue University in 2003. He is currently a Professor at the Department of Electrical and Computer Engineering, Virginia Tech, and the Site Director of the NSF Industry-University Cooperative Research Center (I-UCRC) called Broadband Wireless Access & Applications Center (BWAC). His research interests include dynamic spectrum sharing, emerging wireless technologies, including the IoT and V2X, wireless security and privacy, and applied

cryptography. His current or recent research sponsors include the National Science Foundation (NSF), National Institutes of Health (NIH), Defense Advanced Research Projects Agency (DARPA), Army Research Office (ARO), Office of Naval Research (ONR), and several industry sponsors. He served as an Executive Committee Member of the U.S. National Spectrum Consortium (NSC) from 2016 to 2018. He is a Fellow of the IEEE for his contributions to dynamic spectrum sharing, cognitive radio networks, and security issues. He was a recipient of the 2017 Virginia Tech College of Engineering Dean's Award for Research Excellence, the 2015 Cisco Faculty Research Award, the 2014 Virginia Tech College of Engineering Faculty Fellow Award, the 2008 NSF Faculty Early Career Development (CAREER) Award, the 2008 Hoeber Excellence in Research Award, and the 1998 AT&T Leadership Award. He is currently serving on the editorial boards of a number of IEEE journals, and is actively involved in the organization of a number of flagship conferences. He is currently serving as the Steering Committee Chair of the IEEE International Symposium on Dynamic Spectrum Access Networks (DySPAN).



William Lehr received the B.S., B.A., and M.S.E. degrees from the University of Pennsylvania, the M.B.A. degree in finance from The Wharton School, The University of Pennsylvania, and the Ph.D. degree in economics from Stanford University. He is currently an Internet and Telecommunications Industry Economist and a Research Scientist at the Computer Science and Artificial Intelligence Laboratory (CSAIL), Massachusetts Institute of Technology (MIT), where he is also with the Advanced Network Architectures Group. His research focuses

on the economic implications of ICT technologies for public policy, industry structure, and the evolving Internet ecosystem. In addition to his academic work, he advises public and private sector clients in the U.S. and abroad on ICT strategy and policy matters.